Title

p100/IκBδ sequesters and inhibits NF-κB through kappaBsome formation

Journal

Proceedings of the National Academy of Sciences of the United States of America, 111(45)

ISSN

0027-8424

Authors

Tao, Zhihua
Fusco, Amanda
Huang, De-Bin
et al.

Publication Date

2014-11-11

DOI

10.1073/pnas.1408552111

Peer reviewed

p100/IκBδ sequesters and inhibits NF-κB through kappaBsome formation

Zhihua Tao[a,1], Amanda Fusco[a,1], De-Bin Huang[a,1], Kushol Gupta[b], Daniel Young Kim[a], Carl F. Ware[c], Gregory D. Van Duyne[b], and Gourisankar Ghosh[a,2]

[a]Department of Chemistry and Biochemistry, University of California, San Diego, La Jolla, CA 92093; [b]Department of Biochemistry and Biophysics, University of Pennsylvania, Philadelphia, PA 19104; and [c]Infectious and Inflammatory Diseases Center, Sanford–Burnham Medical Research Institute, La Jolla, CA 92037

Edited by Michael Karin, University of California, San Diego School of Medicine, La Jolla, CA, and approved September 19, 2014 (received for review May 9, 2014)

Degradation of I kappaB (κB) inhibitors is critical to activation of dimeric transcription factors of the NF-κB family. There are two types of IκB inhibitors: the prototypical IκBs (IκBα, IκBβ, and IκBε), which form low-molecular-weight (MW) IκB:NF-κB complexes that are highly stable, and the precursor IκBs (p105/IκBγ and p100/IκBδ), which form high-MW assemblies, thereby suppressing the activity of nearly half the cellular NF-κB [Savinova OV, Hoffmann A, Ghosh G (2009) *Mol Cell* 34(5):591–602]. The identity of these larger assemblies and their distinct roles in NF-κB inhibition are unknown. Using the X-ray crystal structure of the C-terminal domain of p100/IκBδ and functional analysis of structure-guided mutants, we show that p100/IκBδ forms high-MW $(IκBδ)_4$:$(NF-κB)_4$ complexes, referred to as kappaBsomes. These IκBδ-centric "kappaBsomes" are distinct from the 2:2 complexes formed by IκBγ. The stability of the IκBδ tetramer is enhanced upon association with NF-κB, and hence the high-MW assembly is essential for NF-κB inhibition. Furthermore, weakening of the IκBδ tetramer impairs both its association with NF-κB subunits and stimulus-dependent processing into p52. The unique ability of p100/IκBδ to stably interact with all NF-κB subunits by forming kappaBsomes demonstrates its importance in sequestering NF-κB subunits and releasing them as dictated by specific stimuli for developmental programs.

IκB | NF-κB | transcription | structure | kappaBsome

IκB family members carry out distinct cellular functions likely through their ability to inhibit a specific set of NF-κB (1–3). For example, whereas IκBα specifically inhibits the p50:RelA heterodimer and IκBβ targets the RelA:cRel heterodimer (4), IκBε is thought to inhibit the RelA and cRel dimers (5). p105/IκBγ and p100/IκBδ, on the other hand, constitute a different class of inhibitors. These two proteins play dual roles; they not only serve as precursors of the NF-κB proteins p50 and p52 but also inhibit NF-κB including its processed products. Upon specific stimuli, prototypical IκBs and IκBγ undergo phosphorylation by IkappaB kinase, which is followed by their complete degradation and concomitant release of activated NF-κB. These pathways are commonly known as the canonical NF-κB activation pathways (6, 7). Stimulus-dependent generation of p52 from p100/IκBδ constitutes an alternative paradigm of NF-κB signaling, which is referred to as "noncanonical signaling" (8–10). This processing must be controlled such that a significant level of unprocessed molecules remains to maintain normal cellular activity (11). Suppression of IκBδ activity while retaining the processed product p52 results in high and persistent levels of nuclear NF-κB and in uncontrolled activation of many genes resulting in the aberration of several developmental programs such as osteoclastogenesis, B- and T-cell maturation, and lymph node formation (12–16). An enhanced IκBδ activity is known to induce bone formation whereas an enhanced nuclear NF-κB level leads to bone resorption (12, 17, 18). Because expression of all IκBs, barring IκBβ, is under feedback regulation by NF-κB, postinduction synthesis of these inhibitors dampens the nuclear activity of NF-κB by preventing it from undergoing persistent gene activation (3). This negative feedback loop is critical to involvement of IκBδ in long-lasting signals to pathogenic stimuli such as lipopolysaccharides; in contrast, other IκBs mediate signals for rapid NF-κB activation (19, 20).

Extensive works have revealed the biochemical mechanism of interactions between NF-κB and prototypical IκBs (21). In these cases, one NF-κB dimer interacts with one IκB molecule where the ankyrin repeat domain (ARD) of IκB makes noncontiguous contacts with the NF-κB dimer. The nuclear localization sequence (NLS) of one NF-κB subunit interacts at the N-terminal AR of IκBα, and the C terminus of IκBα near the PEST sequence extends underneath the dimerization domain of NF-κB, resulting in low picomolar affinity and extremely low dissociation rates (22–25). The N-terminal signal response domain of IκB remains free for phosphorylation and ubiquitination, suggesting that IκB might degrade while it is bound to NF-κB. Our work on p105:IκBγ revealed that p105 forms a dimer sequestering two NF-κB monomers although the precise mode of how p105 assembles with two NF-κB monomers is unknown. Interestingly, the C-terminal domain (CTD) of p105/IκBγ fails to bind RelB, although p50, the processed product of p105, interacts with RelB to form the p50:RelB heterodimer (26). We also showed that, like p105, p100 forms a large complex of unknown stoichiometry with NF-κB. However, almost nothing else is known about the mode of NF-κB

Significance

NF-κB activation pathways program cells to induce various activities including survival and inflammation. NF-κB activation requires inhibitor IκB degradation. Two of the IκB proteins, p100 and p105, are also the precursors of two NF-κB proteins, p52 and p50. The mechanism by which the p100 inhibits NF-κB remains elusive. The X-ray structure of the C-terminal domain of p100 reveals tetrameric organization and an essential function of tetramerization in sequestering four NF-κB molecules in a subunit-independent manner. Such broader nonspecific NF-κB inhibition by p100 contrasts with the functions of other IκB proteins. A host of genetic mutations linked to excessive p100 processing derail homeostatic NF-κB activity. Our work provides a molecular framework to understand homeostatic regulation of p100 function.

Author contributions: Z.T., A.F., and G.G. designed research; Z.T., A.F., D.-B.H., K.G., and D.Y.K. performed research; C.F.W. and G.D.V.D. contributed new reagents/analytic tools; Z.T., A.F., and D.-B.H. analyzed data; and A.F. and G.G. wrote the paper.

The authors declare no conflict of interest.

This article is a PNAS Direct Submission.

Data deposition: The atomic coordinates and structure factors have been deposited in the Protein Data Bank, www.pdb.org (PDB ID code 4OT9).

[1]Z.T., A.F., and D.-B.H. contributed equally to this work.

[2]To whom correspondence should be addressed. Email: gghosh@ucsd.edu.

This article contains supporting information online at www.pnas.org/lookup/suppl/doi:10.1073/pnas.1408552111/-/DCSupplemental.

inhibition by p100/IκBδ at the molecular levels. This study provides mechanistic insight into the inhibitory function of p100/IκBδ against a broad class of NF-κB factors. We have determined the X-ray crystal structure of the CTD of p100. This structure, in combination with biochemical and cellular studies, allows us to propose a model of how four molecules of p100 assemble with four NF-κB monomers, forming a 4:4 complex, which we refer to as "kappaBsome." We further show that the large molecular assembly is required for p100 to function as an inhibitor.

Results and Discussion

Earlier biochemical analysis revealed that p105/IκBγ associates with NF-κB monomers, forming complexes with 2:2 stoichiometry (27). However, no such details of p100/IκBδ oligomer formation or its functional consequence are known. It is known that the CTD of p100 retains, at least in part, the inhibitory effect exhibited by the full-length p100 (19, 28). To address the oligomerization possibilities and inhibitory mechanism, we generated several deletion mutants of the p100-CTD and tested their oligomerization tendencies by size-exclusion chromatography. Although CTD(407–899) and CTD(407–765) formed oligomers, CTD(482–899) eluted as a smaller-molecular-weight (MW) protein. This suggested that a small N-terminal segment of CTD is responsible for oligomerization (Fig. 1 *A* and *B*). To define the molecular basis for CTD oligomerization, we crystallized CTD (407–765), CTD(407–850), and CTD(407–899). The CTD(407–765) and CTD(407–850) crystals diffracted to resolution of 3.3 and 3.5 Å, respectively (Table S1). We did not continue the structural work of CTD(407–850) because the segment beyond residue 765, which includes the death domain, was found to be disordered. As predicted from the sequence analysis, the X-ray structure of CTD (407–765) revealed an ARD comprising seven ARs, each AR containing two helices and a β-hairpin (Fig. 1*C* and Fig. S1). A long acidic insert (residues 702–725) between AR6 and AR7 is disordered. The N-terminal segment preceding the ARD folded into a helix-turn-helix (HTH) motif, composed of a long 30-residue-long helix (α1) connected to a shorter helix (α2) by a tight 3-residue turn.

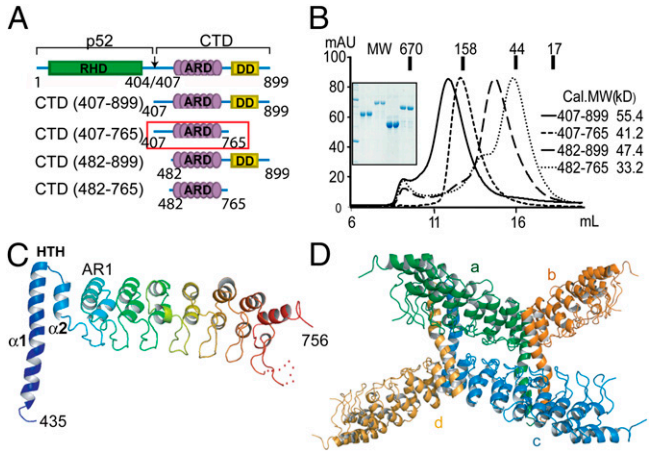

Fig. 1. X-ray structure reveals tetrameric arrangement of the CTD of p100. (*A*) A schematic representation of the domain organization of p100/IκBδ (p100 and IκBδ are identical entity where p100 is the polypeptide and IκBδ is the biochemical activity of p100). CTD fragments used in this study are highlighted, and the crystallized construct is marked with a red box. The tentative site of processing is indicated by an arrow (37). (*B*) Elution profiles of p100-CTDs (407–899, 407–765, 482–765, and 482–899) from an analytical Superdex 200 size-exclusion column with overlaid MW standards. MWs of each CTD are indicated. (*C*) Ribbon diagram of a protomer highlighting the HTH motif and AR domains. AR1 is marked. (*D*) Ribbon representation of the tetrameric assembly of CTD (four protomers are colored differently and labeled as a, b, c, and d).

The asymmetric unit contained only one CTD molecule, but two distinct protein–protein interfaces were generated in the crystal lattice (Fig. S2*A*). One such interface involving head-to-head association of two HTH motifs (from molecules a and b) is extensive. The entire HTH motif and AR1 are involved in the dimer formation. Helix α2 nucleates the formation of the dimerization unit by packing against the C-terminal end of helix α1 at one side and the two helices of AR1 on the other. We refer to the HTH/AR1 dimerization unit as the helical dimerization domain (HDD) (Fig. S2 *B* and *C*). This largely hydrophobic interface buries a >3,200-Å^2 surface area and is formed by 30 residues from each subunit. The HTH motif contributes half of these interfacial residues, and AR1 contributes the other half. A cluster of eight residues from the C-terminal portion of helix α1, the turn, and helix α2 (L461, L462, Y464, V466, A468, A470, L473, and L474) interact with seven residues from AR1 (L481, P491, L494, H498, Q500, V503, and Q506) of the opposing subunit. Located at the center of the dimer interface are three hydrophobic side chains, L461, L462, and Y464, making several critical contacts across the interface (Fig. 2 *A* and *B* and Fig. S2). The signature feature of this interaction is the "X- scissor" architecture formed by the symmetrical disposition of the long helices onto each other. This dimer appears to be an elongated single folded unit with an end-to-end distance of 165 Å where the two monomers meet at an angle of 145° (Fig. S2 *B* and *C*).

The second interface, which is also fairly extensive, buries >1,800 Å^2. In this interface, the helix α1 of the subunits of an X-scissor dimer interacts with AR1-2–3 of one subunit of a second X-scissor dimer (Figs. 1*D* and 2*D*). This interface is uneven in nature with fewer specific contacts that are mostly hydrophobic in nature. The two interfaces together generated an interesting twofold symmetric tetramer that adopts the shape of a parallelogram. In this tetramer, one of the subunits in each dimer is not involved in tetrameric contacts, suggesting different functional consequences for the two types of ARDs in the tetramer. Overall, the tetramer interface involves a total of 11 residues from the HTH/AR1 dimerization domain and 9 residues from AR2/3 containing both nonpolar and polar contacts (Fig. 2 *C* and *D*). As expected, we found that residues at the dimer interface are highly conserved between p100 and p105; however, strikingly, these two molecules share no sequence similarity at the tetramer interface. This explains why p105 forms a 2:2 complex with NF-κB subunits whereas p100 can potentially form 4:4 complexes with NF-κB subunits (Fig. S1). These observations also explain how p100 can associate with p105 through their homologous HDD.

To test whether CTD dimeric interfaces and underlying interactions observed in the structure are real, we generated two mutants. A Tyr464Asp single mutant (DM1) was designed to disrupt the dimer interface 1. The DM1 eluted as a low-MW single species when run in a size-exclusion column, confirming the essential role of Tyr464 in dimer formation (Fig. S3*A*). Multi-angle light scattering (MALS) allowed us to calculate the MW of DM1 to be 41 kDa, which correlates with the monomeric state of the protein. In contrast, WT CTD(407–765) elution profile indicated multiple species of MW ranging between 41 and 141 kDa. The dominant peak tallied with the dimeric species, and a small but distinct peak corresponding to a tetramer was observed. A second double mutant (TM2; Tyr446Ser and Arg449Ser) at the tetramer interface did not show any peak corresponding to a tetramer but appeared to retain some propensity to dimerize because the peak contained species ranging from MW 41 to 57 kDa. These results indicate that CTD might form a weak tetramer in solution that is further stabilized in the crystal (Fig. S3*A*). Next we tested if the N-terminal p52 domain of p100 plays any role in stabilizing the tetramer. MALS of full-length p100/IκBδ purified from baculovirus-infected cells indicated that, although it mostly exists as a dimer, a small fraction exists as a tetramer. These data suggest that p52 may help stabilize the p100-CTD tetramer (Fig. 3*A*).

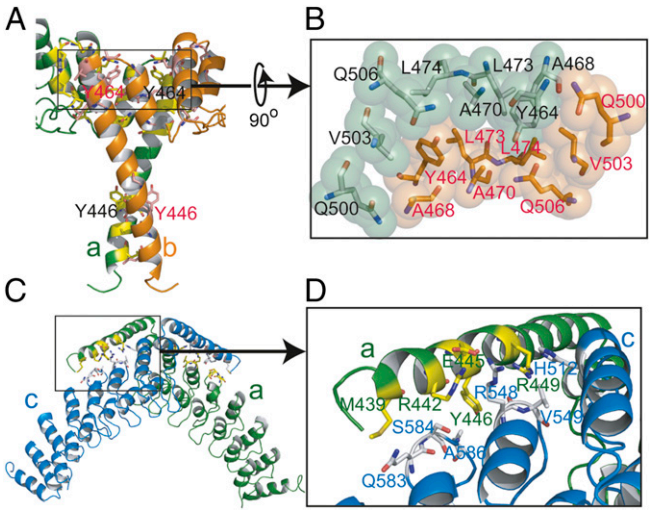

Fig. 2. Interactions of two CTD dimeric interfaces that help form the tetramer. (*A*) Dimerization interface of HTH-AR1 segments of protomers a and b (nomenclature defined in Fig. 1*D*). Y464 and Y446 located at the dimer and tetramer interfaces, respectively, are highlighted. (*B*) A close-up view of the van der Waals surface representation at the dimeric interface around Y464. (*C*) Ribbon representation of the tetramer interface between protomers a and c. (*D*) A close-up view of interactions between complementary side chains around Y446 at the tetramer interface shown in *C*.

Because we did not succeed in generating a recombinant native IκBδ:NF-κB (RelB/RelA/cRel) complex, we investigated the assembly states of WT and mutant p100 in transiently transfected cells. Flag-epitope–tagged WT p100, DM1, or TM2 mutations were expressed in HEK293 cells. Cytoplasmic extracts from transfected cells were fractionated by size-exclusion chromatography followed by Western blot. As expected, p100-DM1 eluted as a lower-MW protein (fraction #25) relative to the WT (fraction #23), and the peak of TM2 appeared to be in between (fraction #24) (Fig. 3*B*). These experiments were repeated several times, and the general trend was near identical, thus supporting the structural evidence of p100/IκBδ forming a tetramer. We further tested if p100 forms a larger complex with the transcriptionally active NF-κB subunits, RelA, RelB, and cRel. All four proteins were cotransfected, followed by size fractionation of the cytoplasmic extract. We found that all four proteins elute ahead (fractions #20/21) of free p100 (Fig. 3*B*). Together, these observations suggest that free p100/IκBδ exists as a strong dimer with a small propensity to form a tetramer, and this tetramer is stabilized in association with NF-κB subunits. Moreover, we observed that endogenous p100/IκBδ interacts with all three transcriptional-activating NF-κB subunits (RelA, RelB, and cRel) in immunoprecipitation experiments (Fig. S3*B*).

We further measured the binding affinity of CTD(406–899) to the p52 homodimer and the p52:RelB heterodimer using isothermal titration calorimetry. All measurements were done multiple times with different protein preparations. The binding affinity (K_d ~200–600 nM) appears to be three orders of magnitude weaker than that of the IκBα:p50:RelA complex (22) (Fig. 3 *C* and *D*). This suggests that a split p100 molecule (p52+CTD) is unlikely to sequester and inhibit a NF-κB molecule or a processed p52 molecule at the cellular protein concentrations. We also tested the binding affinity of CTD for the p50:RelA heterodimer and found that this heterodimer binds even more weakly to CTD than the p52 homo- or heterodimers. Interestingly, the binding profile of the CTD to the p50:RelA heterodimer and to the p52 homo- and heterodimers is different, suggesting that the p50:RelA heterodimer interacts with intact p100 using a different strategy. This is interesting because a p52:RelB heterodimer or a p52:p52 homodimer bound to the CTD is essentially the p100:RelB or p100:p52 complex. On the other hand, the complex between the p50:RelA heterodimer and CTD is a true ternary complex. Such weak binding affinity between the CTD and p50:RelA heterodimer raises the question of whether the CTD of p100 is able to interact with a preformed NF-κB dimer. Furthermore, the weak binding affinity of the CTD:p52 dimer complexes alludes to the need of a higher-order assembly of p100/IκBδ and multiple (various) NF-κB subunits to gain stability.

To investigate the functional consequences of p100/IκBδ oligomerization, we turned to cell-based experiments. We transduced *p100*$^{-/-}$ 3T3 cells with retroviral expression vectors of WT, DM1, or TM2 mutants of p100. In addition, we also transduced cells with

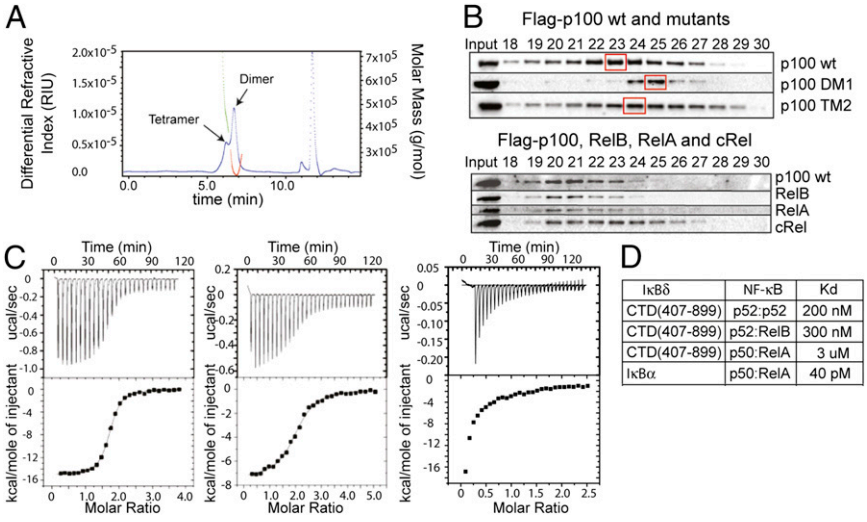

Fig. 3. kappaBsome formation in solution. (*A*) Size-exclusion chromatograph of p100 overlaid with MALS. (*B*) Profile of p100 (WT, DM1, and TM2; *Top*) and p100:RelA:RelB:cRel complexes (*Bottom*) in extracts of 293T cells expressing Flag-p100, Flag-p100DM1, Flag-p100TM2, or Flag-p100, HA-RelA, GFP-RelB, and cRel fractionated through size-exclusion chromatography. (*C*) ITC titration scans showing binding between CTD(407–899), p52(1–406):RelB(1–400), and p50 (39–350):RelA(19-305) heterodimers from left to right. (*D*) Approximate binding affinities of CTD of p100 and NF-κB based on ITC experiments shown in *C*. K_D value of the IκBα:p50:RelA complex is taken from ref. 23 (measurements were done by biomolecular interaction assay using a BIAcore instrument).

DM3 (a Leu461Asp/Leu462Asp/Tyr464Asp triple mutant). The DM3 mutant was expected to have highly defective oligomerization. All mutants were found to be defective in processing of p100 in response to αLTβR (α-LTβ antibody agonist), suggesting that the oligomeric association of p100/IκBδ is critical to appropriate generation of p52 (Fig. 4*A*). We next compared the ability of DM1 and TM2 mutants to inhibit transcriptionally active NF-κB to that of WT by analyzing nuclear NF-κB levels. Consistent with previous reports, EMSA assays showed that the basal DNA-binding activity of nuclear NF-κB in $p100^{-/-}$ 3T3 cells expressing WT p100 was low and that the activity increased upon αLTβR stimulation (19) (Fig. 4*B* and Fig. S4*A*). In contrast, the basal NF-κB activity was high in $p100^{-/-}$ KO cells, indicating the necessity of IκBδ activity in NF-κB inhibition. Cells transduced with DM1 or TM2 mutants also showed higher basal nuclear NF-κB activity than that transduced with WT p100. Moreover, NF-κB DNA-binding activity was not notably enhanced in the DM1 and TM2 transduced cells upon stimulation. Supershift experiments revealed that all three NF-κB subunits, RelA, RelB, and p52, participate in complex formation with DNA (Fig. 4*B* and Fig. S4*B*). This result is surprising because p52 processing is defective in cells expressing the oligomerization-defective mutants of p100. To further test how RelA, RelB, or p52 subunits escape inhibition by the mutants in unstimulated cells, we carried out immunoprecipitation experiments using an antibody against p52/p100. We found that the p100 mutants do not interact with RelA and RelB as efficiently as p100 WT (Fig. S4*C*). Based on these observations, it could be argued that p52 retention by the mutant p100 is also defective. A subcellular fractionation experiment showed the presence of p52 in both the nuclear and the cytoplasmic compartments of unstimulated cells expressing the DM1 or TM2 mutants, and the subcellular distribution did not change in stimulated cells. In contrast, p52 slowly accumulated in the nucleus in stimulated cells expressing WT p100 (Fig. S4*D*). Although the amounts of nuclear p52 do not vary much between WT and DM1 and TM2 cells, the larger quantity of unprocessed p100 in the nucleus of WT cells further suggests that nuclear p52 in WT cells is not free to bind DNA. In contrast, even small amounts of p52 that are generated from the mutants are poorly retained in the cytoplasm or inhibited to bind DNA in the nucleus. These results further suggest that NF-κB inhibitory activity of IκBδ requires its ability to form kappaBsome.

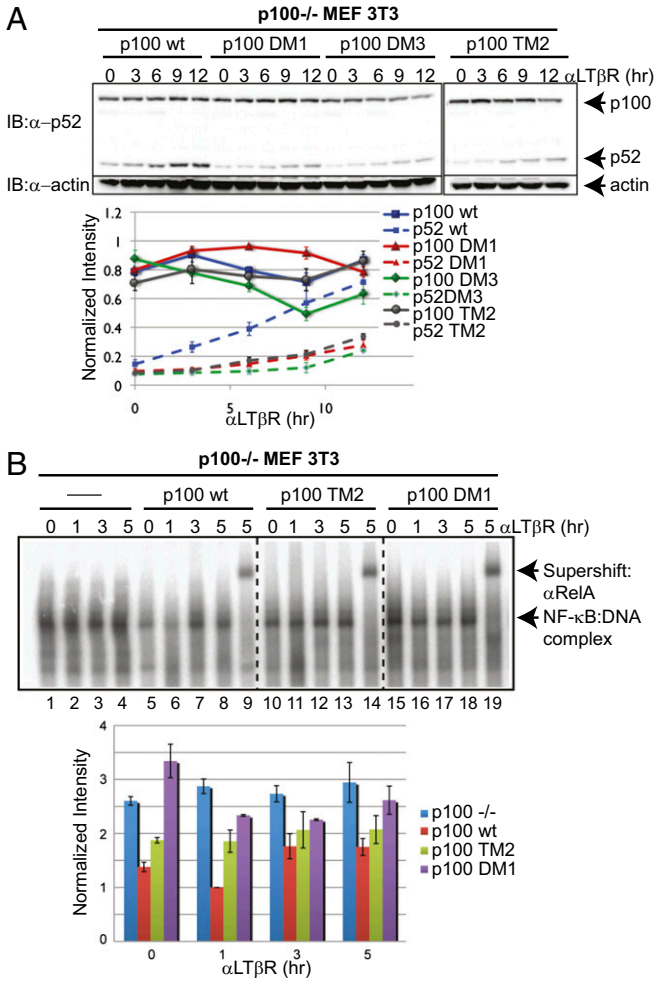

Fig. 4. kappaBsome assembly is essential for function. (*A*, *Top*) Oligomerization is essential for efficient generation of p52. Western blot analyses of $p100^{-/-}$ mouse embryonic fibroblast (MEF) 3T3 whole-cell extracts reconstituted with WT or mutant (indicated) p100 genes prepared at different times after induction. (*Bottom*) Band intensity was quantified and normalized to each loading control. Data are representative of three independent experiments, and the error is determined by SD. (*B*, *Top*) A representative EMSA showing NF-κB DNA-binding activities of extracts from $p100^{-/-}$ 3T3 MEF cells reconstituted with none, WT, or mutant p100 genes with or without α-LTβR treatment. Autoradiograph of the entire gel is shown in Fig. S4*A*. Anti-RelA antibody was used in the supershift experiment. (*Bottom*) The amounts NF-κB:DNA complexes were estimated in imagequant, normalized to background count in each case. Data are representative of three independent experiments, and error was determined by SD.

We next built a model kappaBsomes based on the current structure of the tetrameric CTD and previously determined structures of IκB:NF-κB and NF-κB dimers (23, 25, 29). This model depicts a pathway of the assembly of the monomeric p100:NF-κB (1:1) complex to a dimeric $(p100)_2$:$(NF\text{-}\kappa B)_2$ (2:2) into the final tetrameric 4:4 complex (Fig. 5 *A*–*D*). The intermediate 1:1 and 2:2 complexes are unstable, and the presumed high stability of the 4:4 complex perhaps comes from additional contacts. The disposition of the ARD motif of the CTD in the current structure is such that four NF-κB dimers can engage with the tetramer without any obvious steric collision. Thus, in the context of a tetrameric p100, each of the ARD will have the capability to engage one other NF-κB subunit in addition to its own p52 domain (shown in gray); i.e., an assembly of $(p100)_4$:$(RelA/RelB/cRel)_4$ will be formed. Because p50 and p52 also interact with p100 (19, 30), kappaBsomes containing heterogeneous NF-κB can occur in vivo. This model does not exclude the possibility of a preferentially selective or alternative oligomer formation, and neither does it exclude the possible participation of yet-unknown regulatory factors. Indeed, we have preliminary evidence suggesting a pool of the larger assembly containing both p100 and p105. p105 as a sole inhibitor cannot form the 4:4 complex because it undergoes constitutive processing into p50 and the processed product remains bound to p105. Thus, with two of the CTDs removed, the p105:p50 complex forms a larger $(p105:p50)_2$ assembly by dimerization through HDD (27). Our model also allows us to envision how mutations at the dimerization and tetramerization interfaces disassemble the larger complexes (Fig. 5*E*).

Work presented here shows that IκBδ is a unique inhibitor of the IκB family. It uses NF-κB–assisted oligomeric assembly to inhibit all NF-κB subunits. Although IκBγ and IκBδ possess several similarities in primary structures, IκBγ-mediated kappaBsomes are smaller in size (2:2). It is likely that the inability of IκBγ to tetramerize prevents it from forming the larger oligomer in association with NF-κB. The key residues responsible for IκBδ dimer formation are conserved in IκBγ, suggesting a common mechanism of dimerization between these two molecules (Fig. S1). However, residues at the tetramer interface of IκBδ are not conserved in IκBγ. Although IκBδ exhibits only a low propensity to tetramerize on its own, it forms a stable tetramer when

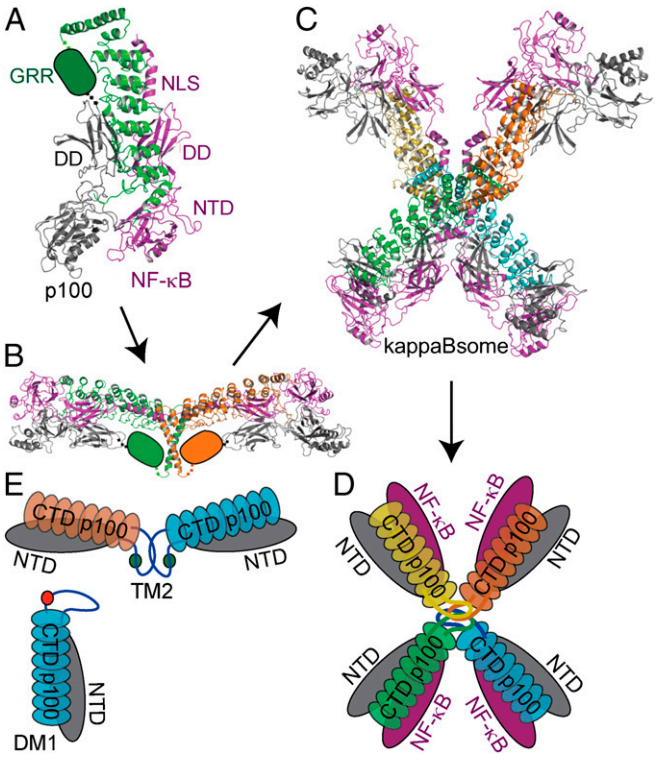

Fig. 5. A model of kappaBsome formation. (*A*) A model of p100 binding to a monomeric NF-κB based on known structures of IκB:NF-κB complexes. In this model, the intact glycine-rich region (GRR) shown in green connects p100-RHD (p52) to p100-CTD. Different domains of NF-κB are denoted (DD, dimerization domain; NTD, N-terminal domain; and NLS, nuclear localization signal). (*B*) The pathway of the kappaBsome formation where two molecules of p100 or p105 form dimers, and each protomer in the dimer associates with a NF-κB protomer. (*C*) In the case of p100, two dimers associate to form the octameric complex. In the case of p105, dimers fail to further associate to form a tetramer. (*D*) A schematic of the octameric p100:NF-κB complex generated based on the model shown in *C*. (*E*) A cartoon presentation of the assembly defects of the p100 DM1 mutant (site of mutation denoted by a red circle) and TM2 mutant (site of mutation denoted by two green circles).

associating with NF-κB monomers. We previously showed that RelB does not interact with the IκBγ (26), which suggests that RelB might play a special role in stabilizing the IκBδ-kappaBsomes. Future studies will explore if and how RelB plays a discriminatory role in kappaBsome formation.

The distinct ability of p100/IκBδ to simultaneously inhibit all NF-κB subunits sheds light on NF-κB regulation by IκBδ, both pre- and postinduction. Many physiological programs require all three NF-κB activators to be relieved from inhibition simultaneously so that they can regulate their respective targets on time. Similarly, efficiency of postinduced inhibition of NF-κB by p100 is determined by the stability of the inhibited complexes. Broad spectrum NF-κB inhibitory activity, release of active NF-κB, and a controlled processing activity of p100 place it at the center of several tissue developmental programs. In these developmental programs, different dimers are required to activate and repress complex sets of genes over a long timescale. Therefore, it is not surprising why mis-regulation of p100/IκBδ is linked to various diseases including cancer (31–33).

Materials and Methods

Protein Purification, Crystallization, Data Collection, and Structure Solution. Human p100/IκBδ CTD fragments were subcloned into pET21d vector with an N-terminal His tag and a tobacco etch virus (TEV) protease cleavage site. The proteins were overexpressed in *Escherichia coli* Rosseta2 BL21(DE3) cells. Cells were grown to an OD_{600} of ∼0.2–0.4 followed by induction with 0.4 mM isopropyl β-D-1-thiogalactopyranoside and continued growth overnight at room temperature. Soluble extract was prepared by sonication of the cell pellet suspended in 150 mM NaCl and 25 Tris·HCl 7.5 and purified using nickel affinity chromatography. The polyhistidine tag was removed by TEV cleavage, and the untagged proteins were further purified by size-exclusion chromatography using a Superdex 200 gel filtration column. Crystals were grown by the hanging drop vapor diffusion method at 20 °C where 12 mg/mL of protein (in 25 mM Tris·HCl, pH 7.5, 100 mM NaCl, 5% (vol/vol) glycerol, and 1 mM DTT) was mixed with an equal volume of reservoir solution that contained 100 mM MES, pH 6.5, 1.4 M ammonium sulfate, and 7.5% 1, 4-dioxane. Before data collection, crystals of CTD(407–765) and CTD (407–850) were soaked for about 1 min in a cryoprotectant buffer containing the original reservoir solution plus 28% glycerol and flash-cooled under liquid nitrogen. X-ray diffraction data were collected at the APS ID24 synchrotron source. The diffraction patterns revealed that both the crystals belong to the hexagonal space group $P6_322$ with similar unit cell: a = b = 196.67, c = 68.46 Å (CTD 407–765). X-ray diffraction data were integrated and scaled to a 3.3- and 3.5-Å resolution, respectively, using HKL2000 (34). The data processing statistics are included in Table S1.

The structure of CTD(407–765) was determined by molecular replacement using MOLREP (35), with the structure of Bcl3 (Protein Data Bank ID 1K1A) as the search model. The orientation and position of this initial model were refined by rigid body refinement in CNS(cns_solve_1.3) (36). The structure was further refined using minimization and simulated annealing with a maximum-likelihood target function and a flat bulk-solvent correction using the CNS system. The model rebuilding was performed based on $2F_O$-F_C maps using Xtalview. The N-terminal helixes α-1 and α-2 were built progressively based on electron density difference maps. The R factor was 23.3% and free R factor was 27.2% for the final model. The model was refined against the data of CTD(407–765); no extra density showed up for the death domain because it remained disordered in a big hole (about 100 Å in diameter) in the hexagonal crystal packing (Fig. S2*D*). The detailed results of the refinement are included in Table S1. The coordinates have been deposited in the Protein Data Bank as entry code 4OT9.

Baculovirus Expression of p100. p100/NF-κB2 was subcloned into pFastBac HT-B with an N-terminal His tag and a TEV cleavage site. The proteins were overexpressed in Sf9 Cells using the Bac-to-Bac baculovirus expression system (Invitrogen). Soluble extract of the cells was prepared with sonication of the cell pellet suspended in 20 mM Tris, pH 7.5, 1 M NaCl, 10% glycerol, and 7 mM 2-mercaptoethanol and purified using nickel affinity chromatography. The protein was further purified by size-exclusion chromatography using a Superdex 200 gel filtration column.

Mammalian Cell Culture and Fractionation by Size-Exclusion Chromatography. p100/NF-κB2 and cRel was subcloned into pEYFP-C1 vector (Clontech), which was modified by deleting yellow fluorescent protein and adding an N-terminal FLAG or no tag, respectively. RelB was subcloned into pEGFP-N1 vector (Clontech), and RelA was subcloned into pCMV HA vector. Transfection and fractionation by size-exclusion chromatography were done as previously described (26).

For retrovirus-mediated gene transduction, all of the constructs were cloned into the pBABE vector (pBabe puro), and transgenic cell lines were prepared as described previously (19).

DNA-Binding Assay. EMSAs were done by incubating nuclear extracts with radiolabeled DNA probe containing two HIV-κB sites (19). The supershift analysis was done by incubating the nuclear extracts with the indicated antibodies for 15 min before probe addition.

Mutagenesis. Mutagenesis was carried out following the Stratagene Quick Change procedure. All mutants were verified by sequencing the entire gene.

Multi-Angle Light Scattering. Size-exclusion chromatography for multi-angle light scattering experiments were performed with a Superdex 200 10/300 GL column (GE Healthcare) at 0.5 mL/min at room temperature in 10 mM Na^+/K^+PO4, 100 mM NaCl, and 1 mM DTT. The column was calibrated using the following proteins (Bio-Rad): thyroglobulin [670 kDa, Stokes radius (RS) = 85 Å], γ-globulin (158 kDa, RS = 52.2 Å), ovalbumin (44 kDa, RS = 30.5 Å), myoglobin (17 kDa, RS = 20.8 Å), and vitamin B12 (1,350 Da). Blue-Dextran (Sigma) was used to define the void volume of the column. Absolute molecular weights of the proteins studied were determined using multi-angle light scattering coupled in-line with size-exclusion chromatography. Light scattering from the column eluent was recorded at 16 different angles using a DAWN-HELEOS

MALS detector (Wyatt Technology) operating at 658 nm. The detectors at different angles were calibrated using the small isotropic scatterer horse heart cytochrome C (Sigma) or the monomer peak from BSA (Fisher-Scientific). Protein concentration of the eluent was determined using an in-line Optilab T-rEX Interferometric Refractometer (Wyatt Technology). The weight-averaged molecular weight of species within defined chromatographic peaks was calculated using the ASTRA software version 6.0 (Wyatt Technology) by construction of Debye plots [KC/Rθ versus sin2(θ/2)] at 1-s data intervals. The weight-averaged molecular weight was then calculated at each point of the chromatographic trace from the Debye plot intercept, and an overall average molecular weight was calculated by averaging across the peak.

Isothermal Titration Calorimetry. Isothermal titration calorimetry (ITC) experiments were performed at 25 °C using a MicroCal Omega VP-ITC instrument. For ITC experiments, IκBδ CTD fragments, p52:p52 homodimer, and p52;RelB heterodimer were used. The proteins were dialyzed overnight in the ITC buffer [20 mM Tris (pH 8.0), 50 mM or 150 mM NaCl and 1 mM DTT]. The protein concentrations were in the range of 5 μM in the cell and 50 μM in the syringe. Protein concentrations were determined by absorbance at 280 nm. A typical ITC experiment consisted of a total of 20 injections, where 15 μL of NF-κB was injected into the cell containing either blank or IκBδ CTD. Data were analyzed using a single-binding site model in the MicroCal Origin Software. The stoichiometry of binding ranged from 1.8 to 2.1. Errors for the K_d values were estimated from triplicate measurements. All of the buffers used were made using water purged with nitrogen.

ACKNOWLEDGMENTS. We thank Dr. Raj Rajashankar for help in data collection at the Advanced Photon Source beamline 24ID; Drs. Tapan Biswas, Malini Sen, and Simpson Joseph for critically reading the manuscript and for important suggestions; Dr. Alex Hoffmann for the 3T3 cell lines and for his continuous support; and Nathan Gianeschi for HPLC-coupled MALS. This work is supported by grants from the NIH (AI064326 and GM071862) (to G.G.). Z.T. received support from Tumor Biology Training Grant T32 CA009523.

1. Sun SC, Ganchi PA, Béraud C, Ballard DW, Greene WC (1994) Autoregulation of the NF-kappa B transactivator RelA (p65) by multiple cytoplasmic inhibitors containing ankyrin motifs. *Proc Natl Acad Sci USA* 91(4):1346–1350.
2. Tergaonkar V, Correa RG, Ikawa M, Verma IM (2005) Distinct roles of IkappaB proteins in regulating constitutive NF-kappaB activity. *Nat Cell Biol* 7(9):921–923.
3. O'Dea E, Hoffmann A (2010) The regulatory logic of the NF-kappaB signaling system. *Cold Spring Harb Perspect Biol* 2(1):a000216.
4. Rao P, et al. (2010) IkappaBbeta acts to inhibit and activate gene expression during the inflammatory response. *Nature* 466(7310):1115–1119.
5. Whiteside ST, Epinat JC, Rice NR, Israël A (1997) I kappa B epsilon, a novel member of the I kappa B family, controls RelA and cRel NF-kappa B activity. *EMBO J* 16(6):1413–1426.
6. Heissmeyer V, Krappmann D, Hatada EN, Scheidereit C (2001) Shared pathways of IkappaB kinase-induced SCF(betaTrCP)-mediated ubiquitination and degradation for the NF-kappaB precursor p105 and IkappaBalpha. *Mol Cell Biol* 21(4):1024–1035.
7. Beinke S, Ley SC (2004) Functions of NF-kappaB1 and NF-kappaB2 in immune cell biology. *Biochem J* 382(Pt 2):393–409.
8. Xiao G, Harhaj EW, Sun SC (2001) NF-kappaB-inducing kinase regulates the processing of NF-kappaB2 p100. *Mol Cell* 7(2):401–409.
9. Senftleben U, et al. (2001) Activation by IKKalpha of a second, evolutionary conserved, NF-kappa B signaling pathway. *Science* 293(5534):1495–1499.
10. Sun SC (2012) The noncanonical NF-κB pathway. *Immunol Rev* 246(1):125–140.
11. Tucker E, et al. (2007) A novel mutation in the Nfkb2 gene generates an NF-kappa B2 "super repressor." *J Immunol* 179(11):7514–7522.
12. Novack DV, et al. (2003) The IkappaB function of NF-kappaB2 p100 controls stimulated osteoclastogenesis. *J Exp Med* 198(5):771–781.
13. Weih F, Caamaño J (2003) Regulation of secondary lymphoid organ development by the nuclear factor-kappaB signal transduction pathway. *Immunol Rev* 195:91–105.
14. Ishimaru N, Kishimoto H, Hayashi Y, Sprent J (2006) Regulation of naive T cell function by the NF-kappaB2 pathway. *Nat Immunol* 7(7):763–772.
15. Caamaño JH, et al. (1998) Nuclear factor (NF)-kappa B2 (p100/p52) is required for normal splenic microarchitecture and B cell-mediated immune responses. *J Exp Med* 187(2):185–196.
16. Guo F, Tänzer S, Busslinger M, Weih F (2008) Lack of nuclear factor-kappa B2/p100 causes a RelB-dependent block in early B lymphopoiesis. *Blood* 112(3):551–559.
17. Yao Z, Xing L, Boyce BF (2009) NF-kappaB p100 limits TNF-induced bone resorption in mice by a TRAF3-dependent mechanism. *J Clin Invest* 119(10):3024–3034.
18. Maruyama T, et al. (2010) Processing of the NF-kappa B2 precursor p100 to p52 is critical for RANKL-induced osteoclast differentiation. *J Bone Miner Res* 25(5):1058–1067.
19. Basak S, et al. (2007) A fourth IkappaB protein within the NF-kappaB signaling module. *Cell* 128(2):369–381.
20. Shih VF, et al. (2009) Kinetic control of negative feedback regulators of NF-kappaB/RelA determines their pathogen- and cytokine-receptor signaling specificity. *Proc Natl Acad Sci USA* 106(24):9619–9624.
21. Huxford T, Hoffmann A, Ghosh G (2011) Understanding the logic of IκB:NF-κB regulation in structural terms. *Curr Top Microbiol Immunol* 349:1–24.
22. Bergqvist S, et al. (2006) Thermodynamics reveal that helix four in the NLS of NF-kappaB p65 anchors IkappaBalpha, forming a very stable complex. *J Mol Biol* 360(2):421–434.
23. Huxford T, Huang DB, Malek S, Ghosh G (1998) The crystal structure of the IkappaBalpha/NF-kappaB complex reveals mechanisms of NF-kappaB inactivation. *Cell* 95(6):759–770.
24. Huxford T, Malek S, Ghosh G (1999) Structure and mechanism in NF-kappa B/I kappa B signaling. *Cold Spring Harb Symp Quant Biol* 64:533–540.
25. Jacobs MD, Harrison SC (1998) Structure of an IkappaBalpha/NF-kappaB complex. *Cell* 95(6):749–758.
26. Fusco AJ, et al. (2008) Stabilization of RelB requires multidomain interactions with p100/p52. *J Biol Chem* 283(18):12324–12332.
27. Savinova OV, Hoffmann A, Ghosh G (2009) The Nfkb1 and Nfkb2 proteins p105 and p100 function as the core of high-molecular-weight heterogeneous complexes. *Mol Cell* 34(5):591–602.
28. Naumann M, Nieters A, Hatada EN, Scheidereit C (1993) NF-kappa B precursor p100 inhibits nuclear translocation and DNA binding of NF-kappa B/rel-factors. *Oncogene* 8(8):2275–2281.
29. Malek S, Huang DB, Huxford T, Ghosh S, Ghosh G (2003) X-ray crystal structure of an IkappaBbeta × NF-kappaB p65 homodimer complex. *J Biol Chem* 278(25):23094–23100.
30. Mercurio F, DiDonato JA, Rosette C, Karin M (1993) p105 and p98 precursor proteins play an active role in NF-kappa B-mediated signal transduction. *Genes Dev* 7(4):705–718.
31. Annunziata CM, et al. (2007) Frequent engagement of the classical and alternative NF-kappaB pathways by diverse genetic abnormalities in multiple myeloma. *Cancer Cell* 12(2):115–130.
32. Keats JJ, et al. (2007) Promiscuous mutations activate the noncanonical NF-kappaB pathway in multiple myeloma. *Cancer Cell* 12(2):131–144.
33. Staudt LM (2010) Oncogenic activation of NF-kappaB. *Cold Spring Harb Perspect Biol* 2(6):a000109.
34. Minor W, Cymborowski M, Otwinowski Z, Chruszcz M (2006) HKL-3000: The integration of data reduction and structure solution: From diffraction images to an initial model in minutes. *Acta Crystallogr D Biol Crystallogr* 62(Pt 8):859–866.
35. Vagin A, Teplyakov A (2010) Molecular replacement with MOLREP. *Acta Crystallogr D Biol Crystallogr* 66(Pt 1):22–25.
36. Schröder GF, Levitt M, Brunger AT (2010) Super-resolution biomolecular crystallography with low-resolution data. *Nature* 464(7292):1218–1222.
37. Betts JC, Nabel GJ (1996) Differential regulation of NF-kappaB2(p100) processing and control by amino-terminal sequences. *Mol Cell Biol* 16(11):6363–6371.